frontiers | Frontiers in Cell and Developmental Biology

TYPE Original Research
PUBLISHED 22 May 2025
DOI 10.3389/fcell.2025.1538934

OPEN ACCESS

EDITED BY
Diane Lidke,
University of New Mexico, United States

REVIEWED BY
Müge SERHATLI,
TUBITAK Marmara Research Center (MRC) Climate Change and Life Sciences VP, Türkiye
Tione Buranda,
University of New Mexico, United States

*CORRESPONDENCE
Curtis A. Thorne,
curtisthorne@arizona.edu

RECEIVED 03 December 2024
ACCEPTED 17 April 2025
PUBLISHED 22 May 2025

CITATION
Cabel CR, Guzman BA, Alizadeh E, Li S, Holberg C, Wichaidit C, Cusanovich DA, Paek AL, Thatcher GRJ, Van Doorslaer K, Nargi RS, Sutton RE, Suryadevara N, Crowe JE Jr., Carnahan RH, Campos SK and Thorne CA (2025) Cell-based high-content approach for SARS-CoV-2 neutralization identifies unique monoclonal antibodies and PI3K pathway inhibitors.
Front. Cell Dev. Biol. 13:1538934.
doi: 10.3389/fcell.2025.1538934

Cell-based high-content approach for SARS-CoV-2 neutralization identifies unique monoclonal antibodies and PI3K pathway inhibitors

Carly R. Cabel[1,2], Briana A. Guzman[1], Elaheh Alizadeh[1,2,3], Shuaizhi Li[4], Cameron Holberg[5], Chonlarat Wichaidit[1], Darren A. Cusanovich[1,2,6], Andrew L. Paek[2,7], Gregory R. J. Thatcher[5], Koenraad Van Doorslaer[1,4], Rachel S. Nargi[8], Rachel E. Sutton[8], Naveenchandra Suryadevara[8], James E. Crowe Jr.[8,9,10], Robert H. Carnahan[8,10], Samuel K. Campos[2,4] and Curtis A. Thorne[1,2]*

[1]Department of Cellular and Molecular Medicine, University of Arizona, Tucson, AZ, United States, [2]Cancer Biology Graduate Interdisciplinary Program, The University of Arizona, Tucson, AZ, United States, [3]The Jackson Laboratory for Genomic Medicine, Farmington, CT, United States, [4]Department of Immunobiology, BIO5 Institute, University of Arizona, Tucson, AZ, United States, [5]Department of Pharmacology & Toxicology, R. Ken Coit College of Pharmacy, University of Arizona, Tucson, AZ, United States, [6]Asthma and Airway Disease Research Center, The University of Arizona, Tucson, AZ, United States, [7]Department of Molecular and Cellular Biology, The University of Arizona, Tucson, AZ, United States, [8]Vanderbilt Vaccine Center, Vanderbilt University Medical Center, Nashville, TN, United States, [9]Department of Pathology, Microbiology, and Immunology, Vanderbilt University Medical Center, Nashville, TN, United States, [10]Department of Pediatrics, Vanderbilt University Medical Center, Nashville, TN, United States

The sudden rise of the SARS-CoV-2 virus and the delay in development of effective therapeutics for mitigation made evident a need for ways to screen compounds that can block infection and prevent further pathogenesis and spread. However, identifying effective drugs that are efficacious against viral infection and replication with minimal toxicity for the patient can be difficult. Monoclonal antibodies were shown to be effective, but as the SARS-CoV-2 mutated, these antibodies became ineffective. Small-molecule antivirals were identified using pseudovirus constructs to recapitulate infection in nonhuman cells, such as Vero E6 cells. However, the impact was limited due to poor translation of these compounds in the clinical setting. This is partly due to the lack of similarity of screening platforms to the *in vivo* physiology of the patient and partly because drugs effective *in vitro* showed dose-limiting toxicities. In this study, we performed two high-throughput screens in human lung adenocarcinoma cells with authentic SARS-CoV-2 virus to identify both monoclonal antibodies that neutralize the virus and clinically useful kinase inhibitors to block the virus and prioritize minimal host toxicity. Using high-content imaging combined with single-cell and multidimensional analysis, we identified antibodies and kinase inhibitors that reduce viral infection without affecting the host. Our screening technique uncovered novel antibodies and overlooked kinase inhibitors (i.e., PIK3i, mTORi, and multiple RTKi) that could

be effective against the SARS-CoV-2 virus. Further characterization of these molecules will streamline the repurposing of compounds for the treatment of future pandemics and uncover novel mechanisms viruses use to hijack and infect host cells.

KEYWORDS

HTS, COVID, PI3K-AKT pathway, drug repurposing, HCA

Introduction

The novel coronavirus SARS-CoV-2 initiated the COVID-19 pandemic, spread rapidly, and caused over six million deaths and long-term side effects in many who recovered from infection (Johns Hopkins University JHU, 2020). SARS-CoV-2 is the third of the SARS-related viruses to cause a global pandemic. The first viral pandemic was in 2003 with SARS-CoV, which originated in the Guangdong Province in China in late 2002 (Stadler et al., 2003). The second is the Middle East Respiratory Syndrome (MERS), reported in Saudi Arabia in 2012 (Zaki et al., 2012). As SARS-CoV-2 continues to evolve into new strains and cause disease, it will be a public health challenge for years to come (Soriano et al., 2021a; Soriano et al., 2021b; Graichen, 2021). There is a need to develop a variety of therapeutics that can target and clear infection safely. Previous work has used SARS-CoV-2-positive patient samples to develop antibodies to neutralize the virus (Zost et al., 2020a). While this approach is certainly effective, new variants of the virus arise, the epitopes targeted by the monoclonal antibodies evolve, and neutralizing activity attenuates (Rathnasinghe et al., 2021; Jia and Gong, 2021).

Antiviral small molecules target the function of essential viral proteins but are not safe from evolving viruses (Heyer et al., 2022). Finding specific, efficacious antiviral small molecules has been challenging and takes years of drug optimization (Chen P. et al., 2021; Weinreich et al., 2021; Corti et al., 2021). Repurposing clinically approved drugs, however, has some clear advantages to developing novel drugs. Repurposed drugs are already approved for use or in clinical trials and come with human toxicity profiles (Weisberg et al., 2020; Ashburn and Thor, 2004). Thus, trials to test efficacy against SARS-CoV-2 infection severity can be streamlined. Much work has been done around repurposing known FDA-approved drugs to treat the virus (Dittmar et al., 2021); however, many of these drugs, while effective at clearing the virus, also have significant, dose-limiting toxicities in patients (Ngan et al., 2022). Identifying clinical drugs with antiviral activity without significant host toxicities is a major challenge.

Effective repurposed drugs have been hard to identify, partly because of the simplicity of the drug screening assays for which they are identified. Viral infection and replication assays that capture natural SARS-CoV-2 strain infection and the nuances of host cell viability and health are needed. Many reported high-throughput screens have used pseudovirus systems in non-physiological cells such as Vero cells (Corti et al., 2021; Weisberg et al., 2020; Ashburn and Thor, 2004) or performed as virtual screens (Kandeel et al., 2021). Ideally, high-throughput screening techniques would use live virus and human airway epithelium to measure a compound's effect on live virus levels and account for epithelial cell health.

High-content image-based screening is ideal for capturing many cell-level measurements of infection and host cell health. Here, we performed two high-throughput *in vitro* screens with human lung adenocarcinoma cells and authentic SARS-CoV-2 virus to identify 1) neutralizing antibodies that effectively target and neutralize the virus and 2) kinase small-molecule inhibitors that can be repurposed for use in the clinic against the virus. We identify a new way to screen for viral neutralization and discover monoclonal antibodies and kinase inhibitors (e.g., PI3K) that can block viral entry and replication. The approach we describe proposes a method of evaluating drug effectiveness against SARS-CoV-2 infection while also selecting for minimal host cell perturbation.

Results

Development of high-content SARS-CoV-2 infection assay

Several screens for small-molecule inhibitors of SARS-CoV-2 infection and replication have been performed, yet most have been simple, non-physiological in nature, limiting their impact (Wang et al., 2020; Jeon et al., 2020; Harcourt et al., 2020). We choose to conduct an image-based screen of patient-derived monoclonal antibodies and small-molecule kinase inhibitors in the epithelial lung adenocarcinoma, Calu-3, combined with automated high-content imaging to uncover novel viral replication mechanisms and identify potent and more specific therapeutic strategies (Figure 1). Our approach would allow us to work with true SARS-CoV-2 in human cells and capture viral replication information and small to large host toxicity effects. Caco-2 and Calu-3 cells have been used previously in SARS-CoV-2 research over primary, normal cell lines due to their expression of ACE2 receptors as well as the protease TMPRSS2, which make them permissible to infection (Mautner et al., 2022; Kumar et al., 2021; Baczenas et al., 2021).

Many primary cell lines, including lung-derived ones, are often difficult to expand to the level needed for screening, and normal lung cell lines have low permissiveness to infection. We attempted infection with a human colon polyp organoid monolayer but observed no infection. We found that Calu-3 cells had a higher expression of the ACE2 receptor over Caco-2 cells and thus were chosen to move forward with the screens (Supplementary Figure S1). We used 384-well optically

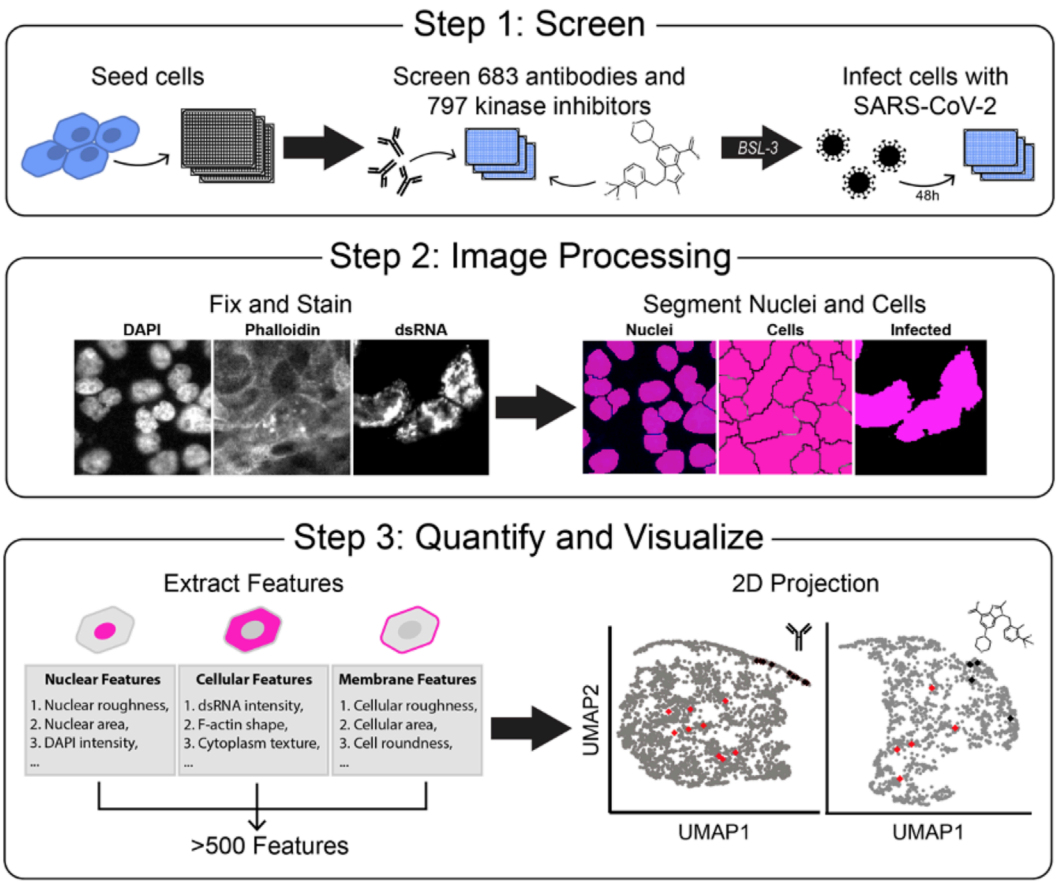

FIGURE 1
Development of a high-throughput SARS-CoV-2 detection screen to identify inhibitors of viral infection. A Overview of experimental design. Step 1: Human lung carcinoma cells are seeded in a 384-well microplate, incubated with treatment, and moved to a BSL-3 facility. Cells are then treated with authentic virus for 48 h. Step 2: Plates are fixed, stained for viral dsRNA, actin (phalloidin), and DNA (DAPI), imaged by fluorescent microscopy, and processed with segmentation software to identify single-cell objects. Step 3: Hundreds of cell features are computationally extracted, and data are visualized in 2D uniform manifold approximation and projection (UMAP) projections.

clear imaging plates and authentic SARS-CoV-2 (strain 2019 n-CoV/USA_WA1/2020) virus to perform this screen. We plated cells in a BSL-2 facility and immediately treated them with small molecules/antibodies before transferring them to the BSL-3 facility and infecting them (Figure 1, Step 1). Mock-infected wells served as our positive control for the desired outcome of infection prevention. Infected-with-vehicle treatment wells served as negative controls and displayed robust viral amplification. The infection and replication were allowed to proceed for 48 h, and then the cells were fixed by full submersion in 4% PFA for 30 min. Plates were moved out of the BSL-3 facility and stained for host cell markers phalloidin (to mark epithelial cell cortex and actin cytoskeleton) and DAPI (to mark nuclei and morphology), as well as dsRNA (to mark infected cells with active, replicating virus). dsRNA is an intermediate product during SARS-CoV-2 viral replication and is a robust marker for infected cells in Calu-3 cells (Bonin et al., 2000; Sola et al., 2015; Li et al., 2021). Combining these three cell stains allowed us to observe how compounds affect viral infection while monitoring effects on host cell number and morphology. To validate our assay, we performed two large-scale screens of neutralizing antibodies and kinase inhibitors to observe the effects on virus replication and the host cell number and morphology.

The screen produced large image sets of cells stained for viral replication (dsRNA), actin cytoskeleton (phalloidin), and nuclear morphology (DAPI). We processed images with Cell Profiler (Carpenter et al., 2006; Lamprecht et al., 2007; Stirling et al., 2021) to segment the images into single-cell objects. Using this software, we took all image sets and segmented each image into single objects guided by the DAPI stain. Then, using the phalloidin stain, we segmented the cell boundaries to distinguish between individual cells. Finally, using the stain for dsRNA, we created a threshold of positive infection to differentiate between areas with SARS-CoV-2 infection and areas without (Figure 1, Step 2). We then extracted measurements of hundreds of cell-level features in three major classes: 1) Morphology, 2) Intensity, and 3) Texture. These features were averaged per well, and uniform manifold approximation and projection (UMAP) dimensionality reduction techniques (Becht et al., 2018; McInnes et al., 2018) were used to project individual drug treatments onto 2-dimensional space for visual evaluation (Figure 1, Step 3). Overall, this approach made for a scalable, 384-well,

automated imaging and analysis format for testing hundreds of compounds.

Neutralizing antibodies reduce SARS-CoV-2 infection in Calu-3 cells

One particularly effective therapeutic strategy for SARS-CoV-2 infection is the delivery of neutralizing monoclonal antibodies (mAbs) developed against the SARS-CoV-2 spike protein that block viral entry. We tested the effects of 683 patient-derived antibodies to block infection of SARS-CoV-2 in human lung adenocarcinoma cells. These antibodies have been developed through B cell enrichment of four COVID-19-positive patients (Zost et al., 2020a; Zost et al., 2020b; Chen E. C. et al., 2021) and tested for binding affinity against the virus spike protein. They were previously classified into five classes representing their binding to the spike protein and whether they cross-reacted with SARS-CoV-1 (Figure 2A): Class I antibodies show binding ability to the ectodomain of trimeric S2 ($S2P_{ecto}$) and the RBD domain of SARS-CoV-2 alone; Class II antibodies bind to the $S2P_{ecto}$ and the RBD domain of SARS-CoV-2 but cross-reacted with the $S2P_{ecto}$ of SARS-CoV-1; Class III bind $S2P_{ecto}$ and the NTD subdomain of SARS-CoV-2 only; Class IV bind $S2P_{ecto}$ of SARS-CoV-2 only with no S1 domain activity; and Class V bind $S2P_{ecto}$ of SARS-CoV-2 and cross-reacted with $S2P_{ecto}$ of SARS-CoV-1. We also tested a Class VI of antibodies that were not shown to interact with the spike protein in SARS viruses from binding assays (Zost et al., 2020a), yet some antibodies from this class could diminish dsRNA signal Calu-3 cells. Their capacity to block authentic virus replication in cells was unknown except for two lead antibodies validated previously (Dong et al., 2021). We tested these antibodies in a dose response of four ten-fold dilutions, infected with an MOI of 1, for 48 h to determine if antibodies were efficacious against an authentic virus challenge.

After fixing, we stained for dsRNA as a measure of viral replication, phalloidin to measure the f-actin of the host cells, and DAPI to visualize the nuclei and imaged using automated microscopy (Figure 2B). We first measured total dsRNA from each of the antibody conditions and plotted them as area under the curve graphs to observe which antibodies reduced the viral burden. Of the antibodies that were tested, the ones in Class I had the most potent response against the virus (Figure 2C). Most of the Class I antibodies reduced the dsRNA intensity to mock-infection levels, while the other classes had fewer antibodies with such potency. Class VI had the largest number of positive hits but also was the largest class of antibodies. Importantly, class VI antibodies were not identified in initial spike protein binding assays, yet we readily observed many apparent potent antibodies in this group. Class VI hits in our screen likely represent false negatives from the previous spike binding characterization or some other unknown mechanism of action. This demonstrates that our high-content and high-throughput assay effectively identifies potent SARS-CoV-2 neutralizing antibodies and could be more sensitive and/or specific than spike protein binding assays.

Multidimensional profiling demonstrates that neutralizing antibodies reduce SARS-CoV-2 infection with minimal effect on the phenotype of Calu-3 cells

Next, we wanted to understand how the phenotype of host cells is affected by antibody treatment and if capturing host morphology measurements enriches "hit" antibody selection. The ideal antibody neutralizes the virus, leaving the host cells indistinguishable from those in uninfected control conditions. As described in Figure 1, we measured over 500 features per cell and performed feature reduction to discard highly correlated measurements. This reduced the features measured down to 150 measurable features used in the analysis. Because highly infected SARS-CoV-2 cells only make up approximately 1% of the Calu-3 cells under our culture conditions (Supplementary Figure S2), we discarded all cells except those with the top 1% of the dsRNA signal. Among this top 1%, we averaged the host cell features at the well level and created a multidimensional profile for each antibody treatment. We performed uniform manifold approximation and projection (UMAP) to reduce dimensionality, which allowed us to plot the results in two dimensions (Figure 3A). In each UMAP, each dot represents a single antibody at a single dose. Two points that are close together share more morphology and dsRNA signal strength than two points that are further away. The 683 antibodies, in general, produced subtle effects on host cell morphology, as might be expected from the fact that antibodies target very specific epitopes. Importantly, the mock controls clustered together (black diamonds, Figure 3A), and the infected controls clustered together (red diamonds). The treatment conditions (gray dots) grouped toward either the infected controls, suggesting those antibodies had poor or no neutralizing activity and the virus distorted host cell morphology, or they grouped with the mock controls, suggesting robust viral neutralization and maintenance of host cell morphology. To understand if this was a concentration-dependent response, we plotted each of the conditions from low to high separately to observe how the antibodies influenced host cell morphology. Visualization of each of the four antibody concentrations separately shows a subtle movement in phenotype from the high infection phenotype toward the uninfected phenotype (Supplementary Figure S3). This confirms that the antibodies do behave in a dose-dependent manner and improve neutralizing capabilities while preserving host morphology as we increase concentration.

To compare dsRNA levels, we colored the UMAP by the median $\log_{10}$-transformed intensity of the dsRNA signal (Figure 3B). The highest dsRNA intensity (yellow) clusters together toward the bottom of the graph, while the uninfected populations (purple) cluster at the top crest, where the mock controls also cluster. We can clearly see a shift from the bottom to the top of the plot as the dsRNA signal decreases; the morphology shifts closer to the mock control (gray diamonds) and away from the infected control (red diamonds). This analysis clearly identifies samples infected with SARS-CoV-2 and clusters them apart from the mock controls. To identify the top antibodies in our screen, we performed a cluster analysis and identified a subgroup of antibodies that co-cluster with mock conditions, consistent with strong viral neutralization activity. When we broke this group down based on spike protein binding class, we see that class I has the highest hit rate of previously defined

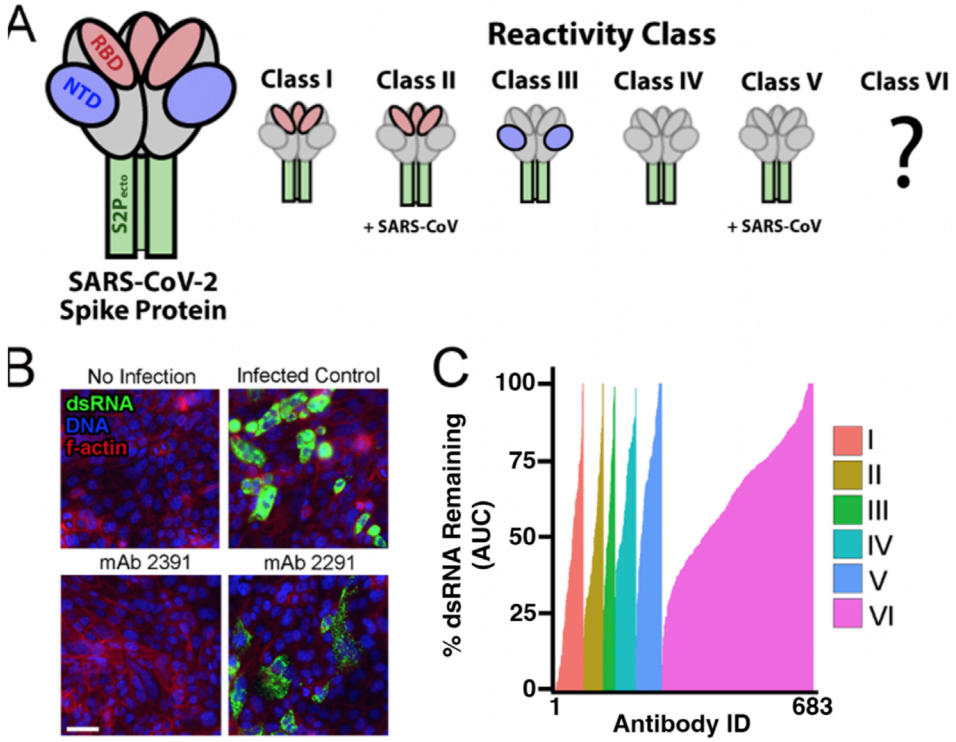

FIGURE 2
Neutralizing antibodies block the virus in Calu-2 cells. **(A)** Description of classes of putative binding properties of patient-derived antibodies to SARS-CoV-2. Red represents the RBD subdomain of the spike protein. Blue represents the NTD subdomain. Green represents the S2P domain. Gray represents parts of the spike protein that are not binding to the antibody. Classes I–V are described in the text and by Zost et al. (2020a). Class VI is an uncharacterized class of antibodies that were isolated from the same SARS-CoV-2 patients as Classes I–V but lacked activity in the secondary spike protein ELISA binding assay. **(B)** Representative images from the antibody screen. No infection represents the Calu-3 cells with mock media and no virus added. Monoclonal antibody (antibody) 2391 was a positive result, showing neutralization of the virus in cells. Antibody 2291 represents a less successful antibody, with clear detection of dsRNA from SARS-CoV-2. Nuclei are stained blue with DAPI. F-actin is stained with phalloidin in red. dsRNA is stained in green. Scale bar = 50 μM. **(C)** Cumulative dsRNA measurements for all antibody treatments sorted by strength of dsRNA signal remaining after ab treatment as percent of infected control. Colors represent the different reactivity classes of antibody targets against the virus. The area under the curve (AUC) is plotted for four increasing concentrations of antibodies. The control concentration has been normalized to a value of 100%.

antibodies classes at 26% (Figure 3C), consistent with many studies showing the RBD domain is the most druggable part of the spike protein (Zost et al., 2020a; Zost et al., 2020b; Hussain et al., 2020).

Kinase inhibitors act to suppress SARS-CoV-2 infection in Calu-3 cells

Kinase inhibitors have been repurposed in the past to act as viral inhibitors for many types of viruses (Weisberg et al., 2020). Tyrosine kinase inhibitors have been identified to block SARS-CoV viruses in Vero E6 cells with minor toxicity to the host cells (Jeon et al., 2020; Weston et al., 2020). In order to test the efficacy of kinase inhibitors against naturally occurring SARS-CoV-2 virus, we tested 796 kinase inhibitors that span the human kinome in our high-content assay with the authentic virus in the same format as the antibody screen described above. We tested two doses, 100 nM and 10 μM, and infected for 48 h with the same immunofluorescent markers (Figure 4A). When we measure mean dsRNA intensity per well, nearly half of the kinase inhibitor library showed some level of reduction in dsRNA staining (Figure 4B). This is likely due to the fundamental role kinases play in cell signaling and cell physiology.

Despite the promise of many kinase inhibitors of reducing apparent viral replication as observed by reduced dsRNA, negative effects on host cells could be responsible for much of this, as kinases are critical for host cell function. To triage compounds that have a deleterious effect on the host cell, we again performed our high-content analysis described in Figure 1. Multidimensional analysis showed that the infected and mock controls were distinct and that kinase inhibitors induced a spread of morphological changes (Figure 4C). Additionally, we saw that movement from infected to mock with increased compound concentration, similar to what we saw with increasing antibody concentrations (Figure 4D). We then evaluated the UMAP with dsRNA median intensity. We confirmed that the cells with lower dsRNA clustered with the mock controls, while the higher dsRNA clustered with the infected control (Figure 4E).

Targeting the PI3K pathway is a putative strategy for SARS-CoV-2 suppression

To evaluate the effect of the kinase inhibitors on the host cell health and morphology, we performed a cluster analysis to

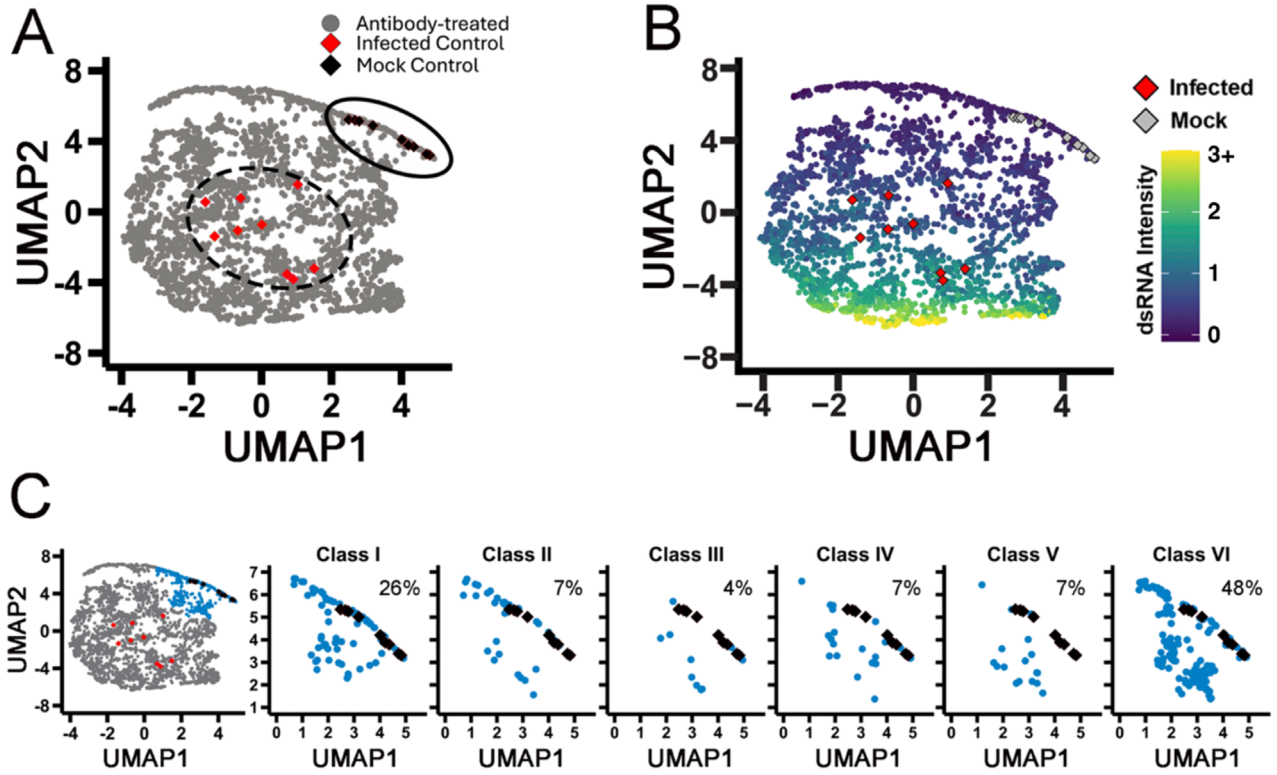

FIGURE 3
High-dimensional profiling shows classes of mAbs that have varying neutralizing activity. **(A)** UMAP of all antibodies. Black diamonds represent mock controls; infected controls are represented by red diamonds, and each gray dot on the map represents a single antibody at a single concentration. **(B)** The UMAP in panel A is recolored as increasing intensity of dsRNA (arbitrary units). Infected controls are represented by red diamonds, and mock controls are represented by gray diamonds. **(C)** Low-virus cluster (blue) broken down by the identified classes. Each graph is labeled with % of class antibodies that had potent neutralizing activity. Classes I and VI had the highest percent of antibodies in the blue cluster compared to other classes.

identify groups that blocked viral inhibition while having minimal effects on cell morphology (Figure 5A). Seven groups of phenotypes were identified, with red cluster #1 representing drug treatment conditions where cells appear healthy and uninfected. When the top hits from single-parameter analysis of dsRNA (Figure 4B) are plotted in UMAP space (Figure 5B), we found that although they reduced the dsRNA signal in cells, only a few showed a healthy host cell phenotype (as denoted by being in the red cluster). Next, we wanted to evaluate how the original two-concentration screen compared to a 12-concentration confirmation study. We hypothesized that an ideal inhibitor that blocks viral replication with minimal host toxicity would phenotypically move into the red group as the treatment concentration increased. Further, the kinase inhibitors blocking viral replication but causing host cell toxicity would not move into the red cluster but away to some other phenotypic cluster. In Figures 5C,D and Supplementary Figure S4, we indicate the two doses of each inhibitor with a gray X. Then, we show low to high doses with an arrow to visualize the directionality of increasing compound concentration in UMAP space. Among the top 33 compounds, our image analysis could identify a wide variety of host cell changes, many of which would be undesirable. An example of this is the drug ibrutinib, a BTK inhibitor (Honigberg et al., 2010; Byrd et al., 2013; Advani et al., 2013), which showed a shift away from the red cluster with increasing concentration (Figure 5C). This suggests that although the inhibitor blocked viral infection, marking it as a top hit, it likely affected the host cell in a toxic way. Indeed, when we challenged the cells with a dose response to block viral infection, it did block the virus in high concentrations but at the cost of significant cell toxicity. Low concentrations had little effect on the virus; at high concentrations, the decrease in dsRNA signal is likely due to a decrease in overall cell host cell viability.

Another example of the reliability of our UMAP analysis is CH5424802, an ALK inhibitor (Sakamoto et al., 2011; Kinoshita et al., 2012). While it reduced dsRNA very well and seemed to pass the cell viability test, looking at morphology, we see that it impacted the nuclei of the host cells by causing blebbing and general toxicity (Figure 5D). This was apparent in the shift in our UMAP data. The high concentration dose ended up in the adjacent yellow cluster, being outside of the target red cluster, showing that the inhibitor affected the host cell negatively.

In contrast to ibrutinib and CH5424802 was GSK2636771, a PI3K inhibitor (Mateo et al., 2017). GSK2636771 showed a shift closer to cluster 1 controls in the two-dose test as well as positive performance in the dose response (Figure 5E). It showed a reduction of dsRNA while having minimal effect on host cell viability and morphology. Unsurprisingly, INK128, an

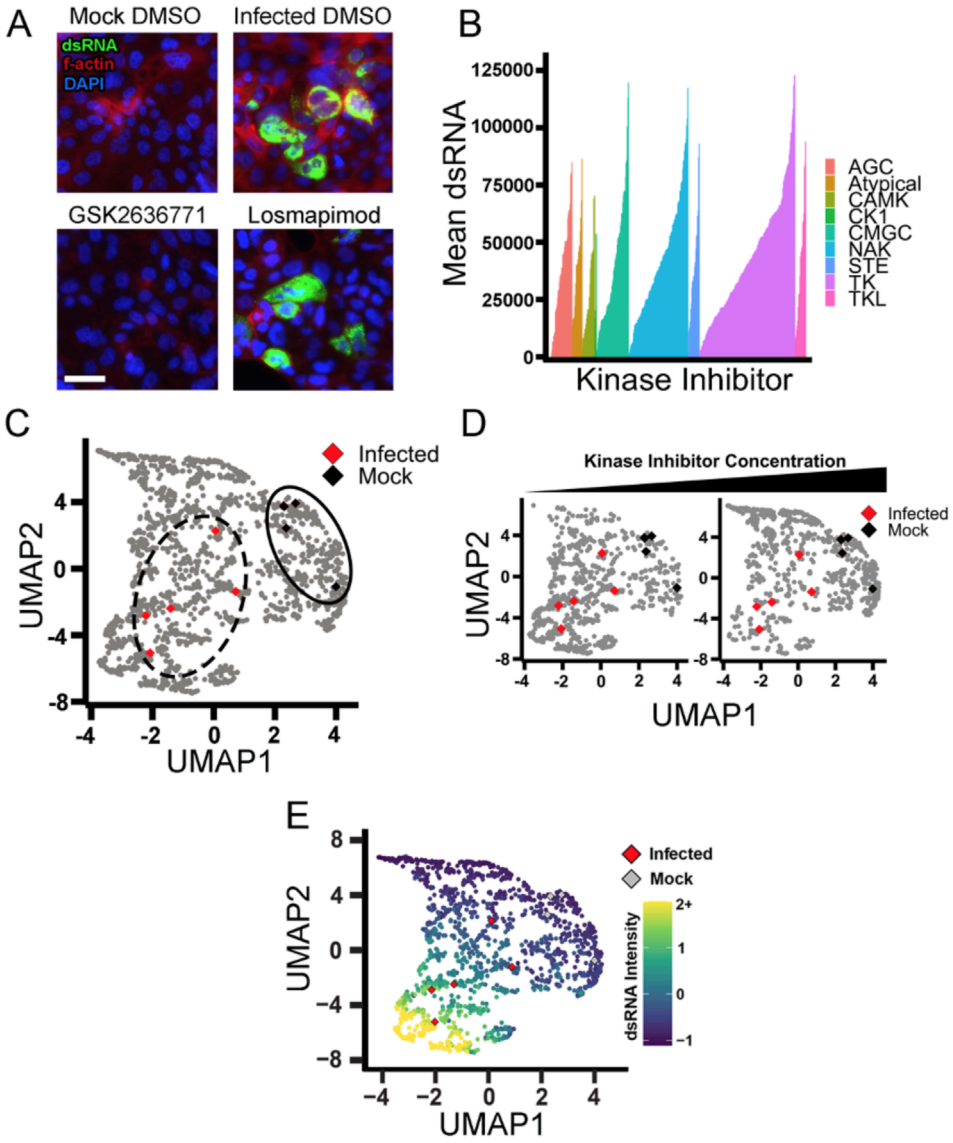

FIGURE 4
Kinase inhibitors from the tyrosine kinase family actively inhibit viral infection. **(A)** Representative images of mock and infected Calu-3 cells with DMSO control. Nuclei are stained in blue DAPI. F-actin is stained with phalloidin in red. dsRNA was stained green, showing active SARS-CoV-2 infection. Scale = 50 μM GSK26367871 represents a kinase inhibitor that reduced infection greatly. Losmapimod represents a kinase inhibitor with poor activity. **(B)** Kinase inhibitors plotted as mean dsRNA, ranked from left to right by the ability to reduce dsRNA. Colors are representative of the branch of the kinome tree they belong to. NAK = not a kinase (inhibitor) and represents compounds whose activity is poorly understood (e.g., flavonoids). **(C)** UMAP of kinase inhibitors compared to infected and mock controls. Each point represents a single kinase inhibitor at a single dose. Infected controls are represented by red diamonds, and black diamonds represent mock controls. **(D)** UMAP of kinase inhibitors separated by concentration. The left plot is 100 nM; the right plot is 10 μM. The shift of the density of points indicates that with an increasing concentration of the kinase inhibitor, the cell phenotype moves closer to the mock control (black diamonds) and away from the infected control (red diamonds). **(E)** The UMAP from **(D)** was recolored to show dsRNA intensity. Red diamonds represent infected controls, and gray diamonds represent mock controls.

mTOR inhibitor, also performed well in our assay by moving into cluster 1 and having little effect on host cell viability (Figure 5F). We observed that for all 33 dsRNA hits, the ones that moved closer to cluster 1 generally exhibited lower toxicity and should be considered strong candidates for repurposing (Table 1, Supplementary Figure S4).

We also wanted to test these top compounds in variants of the SARS-CoV-2 virus. SARS-CoV-2 has shown mutation capability and evasion of drug response, and we hypothesized that using some of the small molecules identified in our screens would still be effective across cell lines as well as viral strains. We tested three compounds in both A549 and Calu-3 lung cells: INK 128 and GSK2636771, which were identified in our screen, and nirmatrelvir (a protease inhibitor) (Owen et al., 2021). We performed a dose–response curve against two additional strains, Omicron BA.1 (B.1.1.529) and Delta (B.1.617.2), and saw similar responses of these small molecule inhibitors against the different strains (Supplementary Figure S5).

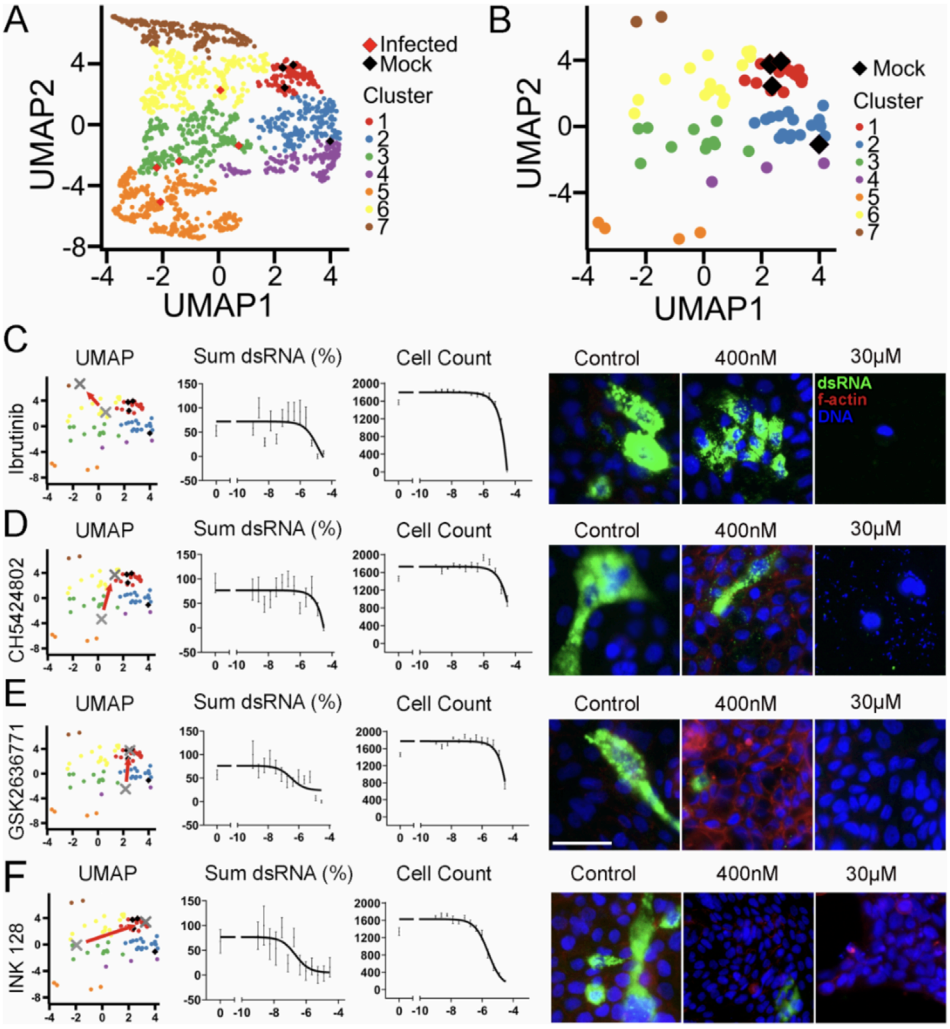

FIGURE 5
PI3K pathway identified as a strategy for SARS-CoV-2 suppression. **(A)** Kinase inhibitor screen hits are grouped by phenotypic clusters. The red cluster 1 groups closely with the mock controls (black diamonds) while the infected controls (red diamonds) expand upon several other clusters. **(B)** The top hits from simple mean dsRNA measurement (Figure 4B) were plotted alone in UMAP. Compounds in the red cluster 1 group still closely resemble the mock controls, yet a wide spread of phenotypes is observed **(C–F)**. The top compounds were retested in a 12-concentration dose–response curve. The gray X indicates the low and high doses from the initial screen. The red arrow points from the low dose to the high dose to emphasize the shift in location UMAP space. Cumulative dsRNA was normalized to percent of response to control. Cell count from the dose–response curve was measured by counting DAPI-stained nuclei. Right side: representative images of the specified kinase inhibitor with low and high concentrations. Nuclei are stained with DAPI in blue, F-actin is stained with phalloidin in red, and dsRNA is stained in green. Scale bar = 50 μM. Error bars represent SEM.

Combination treatment of monoclonal antibodies with small-molecule inhibitors increases the efficacy of neutralization

Due to the success of monoclonal antibodies in the clinic and the promise of our small-molecule inhibitor screen in identifying potential blockers of SARS-CoV-2, we hypothesized that combining both treatments would lead to increased efficacy in neutralizing the virus. To test this, we performed combination treatments using a select few monoclonal antibodies, mAb 2355, mAb 2489, and mAb 2819 and nirmatrelvir to test their synergistic effects against the SARS-Cov-2 WA strain (Figure 6A). Nirmatrelvir is a protease inhibitor compound that targets viral proteases that contribute to viral replication in host cells. This compound has been used to treat SARS-CoV-2 and its variants with success (Aggarwal et al., 2023). Using A549 lung cells, we infected these cells with SARS-CoV-2 and saw robust infection with the virus compared to mock control under DMSO-only conditions (Figure 6B).

To assess whether this compound could synergize with a monoclonal antibody, we tested various concentrations of nirmatrelvir with each antibody in a dose–response curve (Figure 6A) and calculated a synergy score [ZIP synergy model (Ianevski et al., 2022)]. As shown in Figures 6C,D, combination treatment between nirmatrelvir and mAb 2355 and 2489 showed effects with increasing concentrations. Combining nirmatrelvir with mAb 2,355, the effective concentrations of each compound were reduced (Figure 6D, pink boxes) compared to either mAb or compound alone (Figure 6D, orange and green boxes, respectively).

TABLE 1 Top kinase inhibitors from Figure 5 were tested in a dose–response curve. EC_{50} values for dsRNA and cell count are reported. The fold column shows cell count over dsRNA to indicate that a therapeutic window of treatment may exist. Any compound in which the EC_{50} was above 30 μM is reported as >30.*Represents compounds that group with the red cluster from Figure 5 and are the strongest candidates for *in vivo* validation.

Kinase inhibitor	Target	Description	EC50 (μM)		Selectivity index
			dsRNA	Cell count	
CAL-101	PI3K	PI3K inhibitor	0.05213	>30	>575
MLN 2480	Raf	Pan-Raf kinase inhibitor, investigational	0.09983	>30	>300
AXL1717*	IGF1R	IGF-1R inhibitor, orally active	0.003323	0.8195	246.615
Fasudil	ROCK	Protein kinase inhibitor	0.01245	1.221	98.072
GSK2636771*	PI3K	PIK3 inhibitor	0.3188	>30	>94
CYT387	JAK	JAK-1/-2 inhibitor, ATP-competitive	0.02757	2.412	87.486
Trametinib	MEK1/2	MEK1 and MEK2 inhibitor, potent and selective	0.3977	>30	>75
Indirubin	GSK-3	cyclin-dependent kinases and GSK-3β inhibitor	1.137	>30	>26
INK 128*	mTOR	MTOR(TORC-1/-2) inhibitor, potent and selective	0.2132	2.471	11.590
Regorafenib monohydrate	c-RET	Tyrosine kinase inhibitor	6.458	>30	>4
Pazopanib HCl*	VEGFR	VEGFR/PDGFR/FGFR/c-Kit/ c-Fms inhibitor	8.643	>30	>3.5
Ibrutinib	BTK	Bruton's tyrosine kinase (BTK) inhibitor	13.66	>30	>2
Linifanib	VEGFR	VEGFR/PDGFR inhibitor	20.48	>30	>1.4
Vinpocetine	PDE	PDE inhibitor	25.67	>30	>1
XL228*	Aurora Kinase	IGF1R/AURORA /FGFR1-3/ABL/SRC family kinases inhibitor	0.07453	0.0664	0.891
GDC-0084*	PI3K	PI3K and mTOR inhibitor, brain-permeable	1.5	1.309	0.873
AT7519	pan-CDK	Multi-CDK inhibitor	1.231	0.646	0.525
PF-00562271*	FAK	FAK/Pyk2 inhibitor, potent and ATP-competitive	8.596	4.388	0.510
Flavopiridol HCl*	pan-CDK	CDK inhibitor, potent and selective	11.44	0.364	0.032
KX2-391 dihydrochloride	Src	Src kinase inhibitor	8.72	0.1359	0.016
Tivantinib	c-MET	C-Met inhibitor, non-ATP-competitive	>30	2.206	<.07
Ly2608204*	Glucokinase	GK activator	>30	20.86	<0.69
NMS-1286937	PLK	PLK1 inhibitor, orally bioavailable	17.84	0.09155	0.005
TAK-733	MEK1/2	MEK allosteric site inhibitor	>30	>30	NA
CH5424802	ALK	ALK inhibitor, potent and ATP-competitive	>30	>30	NA
Pyridoxine*	Vitamin B6	Vitamin B6	>30	>30	NA
GDC-0068	AKT	Pan-AKT inhibitor, highly selective	>30	>30	NA
Pelitinib*	EGFR	EGFR inhibitor, potent and irreversible	None	5.878	NA
R406	SYK	SYK inhibitor, potent and ATP-competitive	None	1.837	NA
AMG 337	c-MET	MET inhibitor	None	>30	NA

(Continued on the following page)

TABLE 1 (*Continued*) Top kinase inhibitors from Figure 5 were tested in a dose–response curve. EC_{50} values for dsRNA and cell count are reported. The fold column shows cell count over dsRNA to indicate that a therapeutic window of treatment may exist. Any compound in which the EC_{50} was above 30 μM is reported as >30.*Represents compounds that group with the red cluster from Figure 5 and are the strongest candidates for *in vivo* validation.

Kinase inhibitor	Target	Description	EC50 (μM)		Selectivity index
			dsRNA	Cell count	
Epigallocatechin gallate (EGCG)*	PKC	Antioxidant, antiangiogenic, and antitumor agent	None	>30	NA
Genistein	Topoisomerase	ER agonist	None	>30	NA
TG101348*	JAK	JAK-2 inhibitor, potent and selective	None	1.614	NA

*Clusters with mock control in high-dose treatment.

However, none of our drug/antibody combinations reach synergy using the ZIP synergy model. In fact, the combinations showed antagonism. This could be due to the nature of their binding. Both mAbs 2355 and 2819 are Class I antibodies that target the RBD domain, while mAb 2489 is a Class III antibody that binds to the NTD domain, as previously described (Figure 2A). Antagonism was also seen with INK128, a PI3K kinase inhibitor previously tested by our group (Supplementary Figure S6).

Our screen and high-dimensional analysis identified many pathways that may be involved in the hijacking of the host cell machinery by the virus. In particular, we observed many hits from inhibitors upstream and downstream of the PI3K pathway. These include inhibitors of EGFR, PI3K, AKT, GSK3, and mTOR pathways. These signals are critical in cell proliferation and survival and may be critical for viral replication. Our data show that designing a high-throughput screening strategy that accounts for not only reducing a single variate (in our case, dsRNA) but also evaluating the dose-dependent effect, cell viability, and morphological response can benefit drug discovery efforts.

Discussion

Here, we developed a high-throughput and high-dimensional assay for characterizing SARS-CoV-2 infection of human lung cancer cells that captures authentic virus replication and host cell-level features. We tested our assay with monoclonal antibodies and small-molecule kinase inhibitors and identified effective perturbations with minimal host cell toxicity. Our high-dimensional analytical approach allowed us to identify antibodies and kinase inhibitors missed or not reported by other groups. This work highlights a new set of compounds ready to be tested for efficacy in animal models and human clinical trials.

A challenge with the COVID-19 outbreak—and any pandemic—is the need to identify effective therapeutics rapidly. This led researchers to screen bioactive and FDA-approved compounds in simplistic assays that had limited physiological relevance. Vero E6 cell drug screens were common (Wang et al., 2020; Jeon et al., 2020; Harcourt et al., 2020). In hindsight, these kidney epithelial cells derived from African green monkeys were not ideal mimics of human lung physiology. The cells fail to express the necessary proteins to ensure faithful infection and propagation by SARS-CoV-2 as a human cell line would. SARS-CoV-2 pseudovirus systems have emerged as valuable tools for researchers studying coronavirus. These genetically modified viruses retain the key structural features of SARS-CoV-2 but lack the ability to cause a full-blown infection and cause mutations (Funnell et al., 2021). By incorporating the spike protein of the original virus into a harmless viral backbone, the pseudovirus systems mimic the entry process of SARS-CoV-2 into cells. This enables scientists to study the virus's behavior, assess the efficacy of potential treatments or vaccines, and investigate the neutralizing capacity of antibodies. The pseudovirus systems offer a safer alternative to working with the live virus and do not require BSL3 facilities, allowing for adoption among researchers worldwide. The inability of pseudovirus to replicate and spread like the actual virus limits the study of viral dynamics and replication within the host. However, due to their simplified viral structure and the potential for variability between different pseudovirus constructs, findings obtained using pseudovirus systems may not fully capture the complexities of the original virus and may not accurately reflect its behavior (Funnell et al., 2021; Ogando et al., 2020; Davidson et al., 2020).

Our approach using authentic SARS-CoV-2 had challenges as well. Previously, we developed a high-throughput organoid monolayer system for drug screening (Thorne et al., 2018). Initially, we tested SARS-CoV-2 in our colonic organoid model as a screening platform, but we observed exceedingly low infection rates. This could be due to several reasons, such as poor viral receptor expression, host cell interferon response, or structural impairments, such as well-polarized cells and mucus secretion. Using human lung cancer cells and complete SARS-CoV-2 virus also resulted in low infectivity but was sufficient for our study. A caveat of the cell lines we used may be that they do not fully capture the toxicity profile of normal healthy lung epithelium. In addition, single-cell image-based analysis required custom image-processing algorithms that were developed for this study and were thus more time-consuming than simple cell viability or plaque assays. An additional challenge was that using authentic virus required a BSL-3 facility, which not all researchers have access to, and added additional layers to the protocol not needed in a BSL-2 facility. Our study best approximates treating COVID-19 prophylactically, which involves administering preventive measures or medications to reduce the risk of infection before exposure or early in the course of the virus. This approach can help bolster immunity and inhibit viral replication but may not model treatment after a robust infection has occurred.

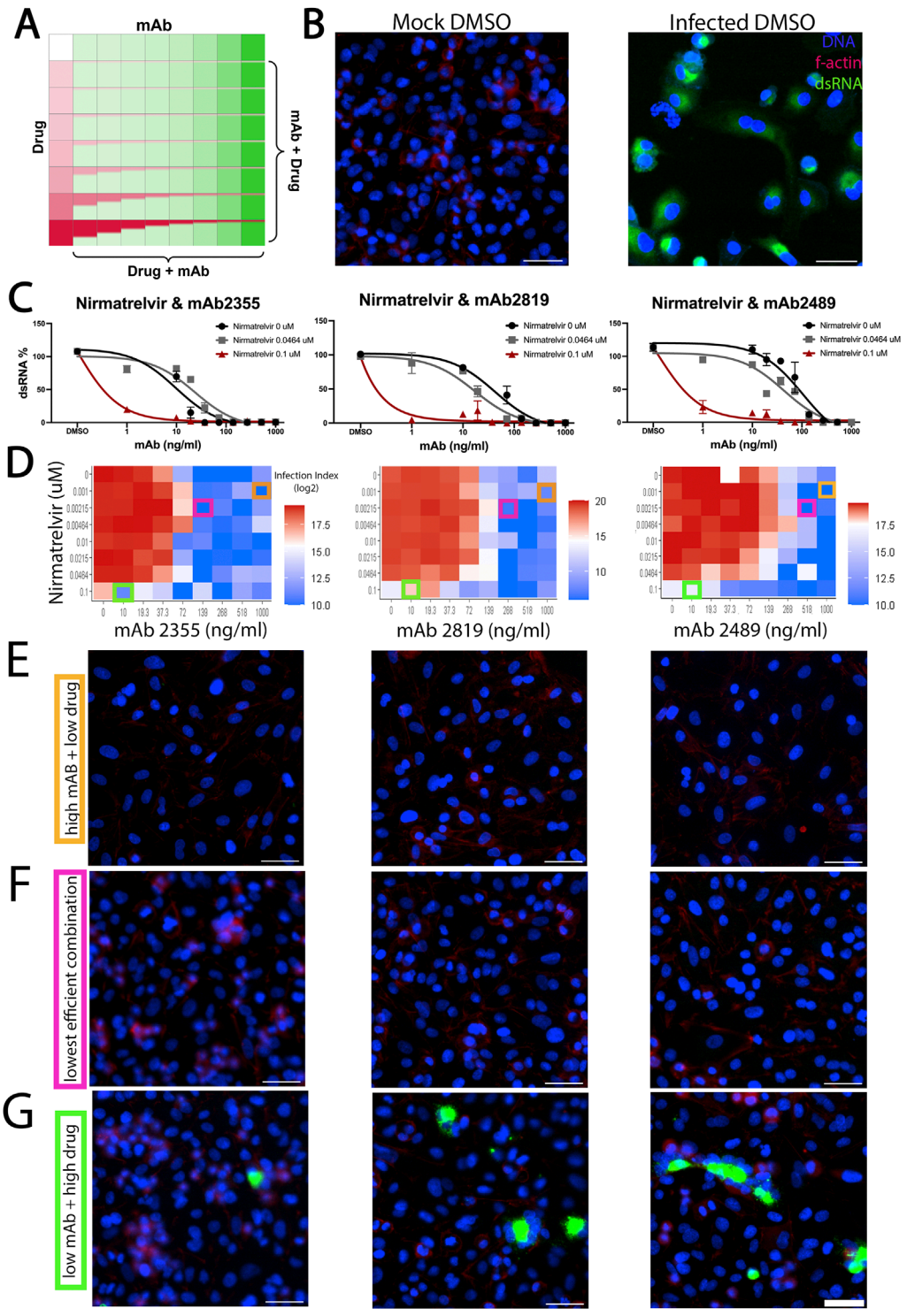

FIGURE 6
Effect of combination treatment of monoclonal antibodies with small-molecule inhibitors on the efficacy of neutralization. **(A)** Schematic of small molecule and antibody combinatorial treatment. Monoclonal antibodies were added in increasing concentrations across the plate, while small molecules were added in reverse concentration at the same time. **(B)** A549 cells were infected with SARS-CoV-2. Mock-"infected" cells were not infected, while DMSO-treated cells were highly infected with SARS-CoV-2. **(C)** Dose–response curve of nirmatrelvir concentrations with selected monoclonal antibodies mAb2355, mAb2819, and mAb 2489. Cumulative dsRNA was normalized to percent of response to control **(D)** Heatmap of infection index of synergy screen. Infection index = Average sum intensity of dsRNA/cell count. Red indicates a higher infection index, while blue represents a lower infection index. Orange, pink, and green boxes around individual data points indicate the respective representative images shown in **(E–G)**. **(E–G)** Representative images of the synergy screen for their respective monoclonal antibodies are shown right above. **(E)** All images correspond to the high monoclonal antibody (10 ug/mL) and low drug concentration (1 nM) used in this screen. **(F)** All images correspond to the lowest efficient combination of monoclonal antibody and drug concentration. **(G)** All images correspond to the low monoclonal antibody (0.1 ug/mL) and high drug concentration (100 nM) combination. DAPI is shown in blue, f-actin is shown in red, and dsRNA as viral infection is shown in green. Scale bar = 50 μM.

Our screening identified hits from both an antibody collection and a kinase inhibitor library. The antibody hits are promising as they could rapidly move into a clinical setting and likely have minimal toxicities. This collection of antibodies already produced two potent neutralizing antibodies that led to Evusheld, an AstraZeneca cocktail globally distributed and accounting for thousands of people treated (Focosi and Casadevall, 2022). However, as new strains of SARS-CoV-2 have evolved, the effectiveness of Evusheld has waned (VanBlargan et al., 2022; Touret et al., 2023).

Our hits can be used as likely candidates for second-line antibody development. Additionally, our high-content assay could be worked into antibody discovery pipelines to rapidly identify efficacious antibodies. We observed hits from all the binding classes of antibodies. From previously defined classes, Class I antibodies are RBD-domain targeted and have the highest hit rate in our screen. This is consistent with the RBD domain's functional role in ACE2 receptor binding (Tai et al., 2020; Chen et al., 2020). Class II and V antibodies were previously shown to have binding to first SARS-CoV-1 and SARS-CoV-2; thus, these hits might have broad efficacy against coronaviruses with similar spike protein structures that infect humans. Class III antibodies are NTD-domain-targeted and had the lowest hit rate in our screen. This is consistent with other reports (Haslwanter et al., 2021; McCallum et al., 2021) that targeting NTD aids viral neutralization, yet the genetic variability of this domain would provide challenges. Class VI hits in our screen likely represent false negatives from the previous spike binding characterization (Zost et al., 2020a). Further structural and biochemical work will need to be done to identify their precise mechanism of action. Finally, little work has been done testing antibody combinations that target the different binding classes. Could an antibody cocktail be identified that is challenging for the virus to evolve away from and lead to longer-lasting clinical efficacy?

Our kinase hits include compounds that target PI3K, EGFR, VEGFR, GSK3, mTOR, and others, some of which have been identified in other studies (Yang et al., 2021; Fattahi et al., 2022; Basile et al., 2022; Londres et al., 2022; Mullen et al., 2021; Liu et al., 2021). Our study identified GSK2636771, a PI3K inhibitor, a clinically useful therapeutic that could move swiftly into clinical trials. Hits from kinase inhibitors, in general, are significant in that 1) their well-characterized mode of action can help tease apart the host signaling pathways involved in viral entry and replication, and 2) they can serve as leads for rapid testing in human clinical trials. A caveat to our study is that it does not account for host immune response, which is a significant aspect of how patients respond to therapeutic intervention of SARS-CoV-2 infection.

Monoclonal antibodies and small-molecule inhibitors are two distinct approaches for targeting SARS-CoV-2, each with its own strengths and weaknesses. mAbs can specifically bind to viral proteins, such as the spike protein of SARS-CoV-2, to neutralize the virus. They have the advantage of high specificity, potency, and the ability to directly block viral entry into host cells with minimal host toxicity. However, mAbs typically require intravenous administration, which limits their accessibility and practicality for widespread use. Further, the emergence of viral variants with mutations in the antibody-binding regions reduces the effectiveness of mAbs and leads to a short life as a clinical option (Touret et al., 2023; McLean et al., 2022).

In contrast to mAbs, small-molecule inhibitors are compounds that interfere with specific viral enzymes or cellular factors necessary for viral replication. They can be orally administered, allowing for easier distribution and patient compliance. Small-molecule inhibitors have a broad spectrum of antiviral activity and can target conserved regions of viral proteins, potentially reducing the impact of viral variants. However, they may lack the high specificity and potency of mAbs, and the resistance to small-molecule inhibitors can develop over time.

By combining the strengths of both approaches, there is potential for synergistic effects and improved therapeutic outcomes. Combinations of mAbs and small-molecule inhibitors can provide a dual mechanism of action, targeting different stages of the viral life cycle. In our study, this combination approach did not show statistically significant synergy. In fact, we observed antagonism. This could be due to the distinct, likely independent mechanism of action (MOA) between the drugs and antibodies. This is potentially important in a clinical setting where a patient may, in fact, be receiving PI3K inhibitors for cancer and may respond poorly to COVID-neutralizing antibody therapy. Future work testing mAbs combinations that target multiple regions of the spike protein or small molecules in synergistic pathways could potentially enhance antiviral efficacy, mitigate the emergence of drug resistance, and offer broader coverage against viral variants. Understanding the complementary strengths and weaknesses of monoclonal antibodies and small-molecule inhibitors is crucial in developing effective treatment strategies against SARS-CoV-2. Continued research and clinical trials are needed to optimize and evaluate the potential of these therapeutic modalities in combating COVID.

Methods

Cell culture

Calu-3 (ATCC, HTB-55) and Caco-2 (ATCC, HTB-37) cells were maintained at 37°C in 5% CO_2 in DMEM with high glucose and 1x GlutaMAX (Invitrogen 35050-061), containing 10% heat inactivated fetal bovine serum (FBS), and 100 U/mL of penicillin–streptomycin. Cells were seeded at 5,000 cells per well in 384 Screenstar microplates (Greiner #781866) and cultured overnight to allow for adherence. The next day, cells were treated with either kinase inhibitors or antibodies before infection for 48 h with the SARS-CoV-2 virus. After 48 h of infection, plates were submerged in 4% paraformaldehyde/sucrose for 30 min and stained for immunofluorescence.

Immunofluorescence

Cells were permeabilized in 0.2% Triton-X in PBS for 10 min. The plates were then blocked with 5% BSA in PBS for 1 h at room temperature before staining. Cells were stained with primary antibody for dsRNA (SCIONS 10010500) at 1:1,000 in BSA/PBS overnight at 4°C in the dark. Cells were washed three times in 0.1% Tween-20/PBS (PBST) for 15 min and incubated in secondary 546 Alexa Fluor anti-mouse 1:1,000 (Fisher A11003) and phalloidin 647 (Biotium 00041) 1:80 for 2 h in the dark at room temperature

in BSA/PBS. Plates were washed three times with PBST and then incubated with 1x DAPI solution in PBS for 30 min at room temperature in the dark. Plates were then washed and stored in PBS. Plates were imaged on a Nikon Eclipse Ti2 automated microscopy system on a ×20 objective. The intensity of dsRNA was measured using NIKON NIS Elements General Analysis software for the Kinase inhibitor assay and neutralizing antibody assay, and cell segmentation was performed using Cell Profiler for the cross analysis and UMAP production. Graphs were produced in Jupyter Notebook using R software.

Viral infection

The USA-WA1/2020 isolate of SARS-CoV-2 was obtained from the World Reference Center for Emerging Viruses and Arboviruses (WRCEVA), and a stock was generated by infecting Vero CCL81 cells for 48 h. The lysate was collected and pelleted to remove the cell debris. Genome sequencing of the virus by Nanopore confirmed the genome sequence to be identical to the GenBank WA1/2020 sequence (MN985325.1), with no mutations in the spike furin cleavage site. The virus was added at a ratio of 1:1 to plates and allowed to incubate at 37°C for 48 h. Plates were submerged in 4% paraformaldehyde/sucrose solution for 30 min to fix cells and decontaminate the plates for removal from BSL-3 facilities. All work with infectious SARS-CoV-2 was performed in an Institutional Biosafety Committee-approved BSL3 facility using appropriate positive-pressure air respirators and protective equipment.

Viral assay for A549 ace2/TMPRSS2 cells

SARS-Cov-2 variants Omicron B.1.1.529 and Delta B.1.617.2 SARS-COV-2 were obtained from BEI. A plaque assay using VeroE6 cells was done to generate viral titers. An MOI of 0.01 was used for WA1, with the viral titer measured at 9e6 pfu/mL. An MOI of 0.03 was used for Omicron BA.1 with a viral titer of 2.4e6 pfu/mL. An MOI of 0.01 was used for Delta B with a viral titer of 4e6 pfu/mL. Cells were infected and left to incubate for 48 h at 37°C/5% CO_2 for 48 h. Note: the calculation is the same for all MOIs used.

After 48 h, the media was removed, and 4% paraformaldehyde phosphate buffer solution (Fujifilm Wako Pure Chemical Corporation) (PFA) was used to fix cells. PFA was added for 30 min per the BSL3 decontamination protocol. The PFA was removed, cells were washed using PBS, and 100 µL of new PBS was added to each well and sent for imaging. Plates were sealed using parafilm.

Neutralizing antibody assay

Cells were seeded at 5,000 cells per well in 384-well microplates (Greiner 789836) and allowed to adhere overnight. A panel of ~500 neutralizing antibodies (Zost et al., 2020a) was added in four ten-fold doses starting at 1:100 on stock antibodies. The cells were treated with SARS-CoV-2 virus for 48 h before being fixed in 4% paraformaldehyde/sucrose solution for 30 min and stained using the methods described. Plates were imaged on a Nikon Eclipse Ti2 automated microscope at ×20 in the same manner as described above. Six frames were captured and analyzed for dsRNA intensity on the whole field, and DAPI was used to measure cell counts. Normalization was performed in the same manner as the kinase inhibitor assay. Raw data were extracted from NIKON NIS Elements software and plotted in R.

Kinase inhibitor assay

Cells were seeded at 5,000 cells per well in 384-well microplates (Greiner 789836) and allowed to adhere overnight. A panel of ~800 kinase inhibitors (ApeXBio L1024) was added in two doses, 10 µM and 100 nM, on the cells. The cells were then treated with SARS-CoV-2 virus for 48 h before being fixed in 4% paraformaldehyde/sucrose solution for 30 min and stained using the methods described. Plates were imaged on a Nikon Eclipse Ti2 automated microscope at ×20. Six frames were captured and analyzed for dsRNA, and DAPI was used to measure cell count. The total dsRNA signal for each inhibitor was measured by segmenting images for the dsRNA threshold, measuring the sum intensity of 546, and dividing by cell count to normalize by well-to-well variation. Wells were then normalized to control wells with the mock infection and treatment with DMSO to account for plate-to-plate variability. Raw data were extracted from NIKON NIS Elements software and plotted in R.

Follow-up confirmation tests were performed with 34 top kinase inhibitors that showed increased efficiency with higher doses and were used as drugs in clinical trials. Those kinase inhibitors were dosed in a 14-dose–response curve. Cells were plated in the same manner as described above, and drugs diluted in DMSO were delivered in a dose curve using a Tecan d300e Digital Dispenser. Dose-response was plotted in GraphPad Prism as the percentage of sum dsRNA to control. Cell count was the average of all wells, and nuclei were counted by DAPI using NIKON NIS Elements software and plotted in Prism. EC_{50} values were calculated in GraphPad. Error bars represent the standard error of the mean of all wells and duplicates.

Combination of neutralizing antibody and kinase inhibitor assay

Cells were seeded at 8,000 cells per well in a 96-well plate (Greiner 655090) and allowed to adhere overnight. One antibody was added per plate in an 8-dose–response curve from 0.01 µg/mL to 10 µg/mL from left to right. At the same time, either INK 128 or nirmatrelvir was added in a 7-dose–response curve from 1 nM to 100 nM. The cells were then treated with the SARS-COV-2 virus for 48 h before being fixed in 4% paraformaldehyde/sucrose solution for 30 min and staining using the methods described above. Plates were imaged on a Nikon Eclipse Ti2 automated microscope at ×20 in the same manner as described above. Six frames were captured and analyzed for dsRNA intensity on the whole field, and DAPI was used to measure cell counts. Normalization was performed in the same manner as the kinase inhibitor assay. Raw data were extracted from NIKON NIS Elements software and plotted in R. Cells were

plated in the same manner as described above, and drugs diluted in DMSO were delivered in a dose curve using a Tecan d300e Digital Dispenser. Heat maps were generated in R.

Segmentation and feature extraction

We used CellProfiler (CP) software to segment images into individual cells. DAPI was used to segment individual nuclei into primary objects. Phalloidin was used to define individual cell borders as secondary objects and use as cell masks. Features were then extracted for individual cells using CP. To calculate the dsRNA features, we used the dsRNA channel and cell mask to quantify different measures based on the intensity of the dsRNA channel within the cell region.

Data preprocessing

Finding the infection rate of the experiment

To find the rate of infection, we plotted the cellular area vs. mean intensity of dsRNA in both mock and infected cells treated with DMSO. The most infected cells, which make up 1% of the cell population, were used to evaluate the response of both monoclonal antibodies and kinase inhibitors in this study. Moving forward, the top 1% of cells in all conditions were evaluated for response.

Normalizing the data

A normalization factor was calculated for each screening set (kinase inhibitor or neutralizing antibody) separately. This factor is the mean of mock DMSO cells in all the plates in each experiment for each feature. The cells were then standardized to make sure all the features were treated the same in the data analysis.

Calculating UMAP

After standardizing the data, we projected it into the UMAP space (arXiv:1802.03426) using the UMAP package in R. Individual points represent the average of a single treatment condition at a single dose. Plots were colored according to increasing dsRNA intensity.

Clustering analysis

Mock DMSO wells in each plate were used as normalization factors. All measures were averaged, and single-cell features were normalized to the mock DMSO condition. We then calculated the mean per condition and projected the data into UMAP space. Using hierarchical clustering, we clustered the data points to determine how the data are scattered in UMAP space and which conditions were found to be next to our controls.

Data availability statement

The original contributions presented in the study are included in the article/Supplementary Material; further inquiries can be directed to the corresponding author.

Author contributions

CC: conceptualization, investigation, writing – original draft, writing – review and editing, data curation, formal analysis, and methodology. BG: data curation, formal analysis, and writing – review and editing. EA: data curation, formal analysis, software, visualization, and writing – review and editing. SL: investigation, methodology, and writing – review and editing. CH: data curation, investigation, and writing – review and editing. CW: formal analysis, software, visualization, and writing – review and editing. DC: visualization and writing – review and editing. AP: resources, supervision, and writing – review and editing. GT: resources and writing – review and editing. KV: conceptualization, funding acquisition, and writing – review and editing. RN: resources and writing – review and editing. RS: resources and writing – review and editing. NS: resources and writing – review and editing. JC: conceptualization, resources, and writing – review and editing. RC: conceptualization, resources, and writing – review and editing. SC: conceptualization, funding acquisition, investigation, methodology, supervision, and writing – review and editing. CT: conceptualization, funding acquisition, investigation, project administration, supervision, writing – original draft, and writing – review and editing.

Funding

The author(s) declare that financial support was received for the research and/or publication of this article. This work was supported by the National Institutes of Health (T32CA009213 to C.R.C., DK103126, GM147128 to C.A.T, GM136853 to S.K.C., GM130864 to A.L.P., and AI157155 to J.E.C.), the ARCS Foundation Phoenix (Theresa F Jennings Award to C.R.C.), the Wellcome Trust, UK (WT223952/Z/21/Z to C.A.T.), the State of Arizona (TRIF to C.A.T., K.V.D.) (TRIF, UA COVID-19 Seed Grant #002196 to S.K.C.), and the Defense Advanced Research Projects Agency (HR0011-18-3-0001 to J.E.C.).

Acknowledgments

We thank the JC, SC, and CT labs for their support and advice. We also thank C. Bradshaw, J. Urlaub, and J. Nikolich-Žugich for use of the BSL-3 facility, propagating the SARS-CoV-2 virus, and providing insights and support.

Conflict of interest

The authors declare that the research was conducted in the absence of any commercial or financial relationships that could be construed as a potential conflict of interest.

Generative AI statement

The author(s) declare that no Generative AI was used in the creation of this manuscript.

Publisher's note

Supplementary material

The Supplementary Material for this article can be found online at: https://www.frontiersin.org/articles/10.3389/fcell.2025.1538934/full#supplementary-material

References

Advani, R. H., Buggy, J. J., Sharman, J. P., Smith, S. M., Boyd, T. E., Grant, B., et al. (2013). Bruton tyrosine kinase inhibitor ibrutinib (PCI-32765) has significant activity in patients with relapsed/refractory B-cell malignancies. *J. Clin. Oncol.* 31, 88–94. doi:10.1200/JCO.2012.42.7906

Aggarwal, N. R., Molina, K. C., Beaty, L. E., Bennett, T. D., Carlson, N. E., Mayer, D. A., et al. (2023). Real-world use of nirmatrelvir-ritonavir in outpatients with COVID-19 during the era of omicron variants including BA.4 and BA.5 in Colorado, USA: a retrospective cohort study COVID-19 during the era of omicron variants including BA.4 and BA.5 in Colorado, USA: a retrospective cohort study. *Lancet Infect. Dis.* 23 (6): 696–705. doi:10.1016/S1473-3099(23)00011-7

Ashburn, T. T., and Thor, K. B. (2004). Drug repositioning: identifying and developing new uses for existing drugs. *Nat. Rev. Drug Discov.* 3, 673–683. doi:10.1038/nrd1468

Baczenas, J. J., Andersen, H., Rashid, S., Yarmosh, D., Puthuveetil, N., Parker, M., et al. (2021). Propagation of SARS-CoV-2 in calu-3 cells to eliminate mutations in the furin cleavage site of spike viruses **13**. *Viruses* 13, 2434. doi:10.3390/v13122434

Basile, M. S., Cavalli, E., McCubrey, J., Hernandez-Bello, J., Munoz-Valle, J. F., Fagone, P., et al. (2022). The PI3K/Akt/mTOR pathway: a potential pharmacological target in COVID-19. *Discov. Today* 27, 848–856. doi:10.1016/j.drudis.2021.11.002

Becht, E., McInnes, L., Healy, J., Dutertre, C. A., Kwok, I. W. H., Ng, L. G., et al. (2018). Dimensionality reduction for visualizing single-cell data using UMAP. *Nat. Biotechnol.* 37, 38–44. doi:10.1038/nbt.4314

Bonin, M., Oberstrass, J., Lukacs, N., Ewert, K., Oesterschulze, E., Kassing, R., et al. (2000). Determination of preferential binding sites for anti-dsRNA antibodies on double-stranded RNA by scanning force microscopy. *RNA* 6, 563–570. doi:10.1017/s1355838200992318

Byrd, J. C., Furman, R. R., Coutre, S. E., Flinn, I. W., Burger, J. A., Blum, K. A., et al. (2013). Targeting BTK with ibrutinib in relapsed chronic lymphocytic leukemia. *N. Engl. J. Med.* 369, 32–42. doi:10.1056/NEJMoa1215637

Carpenter, A. E., Jones, T. R., Lamprecht, M. R., Clarke, C., Kang, I. H., Friman, O., et al. (2006). CellProfiler: image analysis software for identifying and quantifying cell phenotypes. *Genome Biol.* 7, R100. doi:10.1186/gb-2006-7-10-r100

Chen, E. C., Gilchuk, P., Zost, S. J., Suryadevara, N., Winkler, E. S., Cabel, C. R., et al. (2021b). Convergent antibody responses to the SARS-CoV-2 spike protein in convalescent and vaccinated individuals, *Cell Rep.*, 36, 109604 doi:10.1016/j.celrep.2021.109604

Chen, P., Nirula, A., Heller, B., Gottlieb, R. L., Boscia, J., Morris, J., et al. (2021a). SARS-CoV-2 neutralizing antibody LY-CoV555 in outpatients with covid-19. *N. Engl. J. Med.* 384, 229–237. doi:10.1056/NEJMoa2029849

Chen, X., Li, R., Pan, Z., Qian, C., Yang, Y., You, R., et al. (2020). Human monoclonal antibodies block the binding of SARS-CoV-2 spike protein to angiotensin converting enzyme 2 receptor. *Mol. Immunol.* 17, 647–649. doi:10.1038/s41423-020-0426-7

Corti, D., Purcell, L. A., Snell, G., and Veesler, D. (2021). Tackling COVID-19 with neutralizing monoclonal antibodies. *Cell* 184, 3086–3108. doi:10.1016/j.cell.2021.05.005

Davidson, A. D., Williamson, M. K., Lewis, S., Shoemark, D., Carroll, M. W., Heesom, K. J., et al. (2020). Characterisation of the transcriptome and proteome of SARS-CoV-2 reveals a cell passage induced in-frame deletion of the furin-like cleavage site from the spike glycoprotein. *Genome Med.* 12, 68. doi:10.1186/s13073-020-00763-0

Dittmar, M., Lee, J. S., Whig, K., Segrist, E., Li, M., Kamalia, B., et al. (2021). Drug repurposing screens reveal cell-type-specific entry pathways and FDA-approved drugs active against SARS-Cov-2. *Cell Rep.* 35, 108959. doi:10.1016/j.celrep.2021.108959

Dong, J., Zost, S. J., Greaney, A. J., Starr, T. N., Dingens, A. S., Chen, E. C., et al. (2021). Genetic and structural basis for SARS-CoV-2 variant neutralization by a two-antibody cocktail. *Nat. Microbiol.* 6, 1233–1244. doi:10.1038/s41564-021-00972-2

Fattahi, S., Khalifehzadeh-Esfahani, Z., Mohammad-Rezaei, M., Mafi, S., and Jafarinia, M. (2022). PI3K/Akt/mTOR pathway: a potential target for anti-SARS-CoV-2 therapy. *Immunol. Res.* 70, 269–275. doi:10.1007/s12026-022-09268-x

Focosi, D., and Casadevall, A. (2022). A critical analysis of the use of cilgavimab plus tixagevimab monoclonal antibody cocktail (Evusheld) for COVID-19 prophylaxis and treatment viruses **14**. *Viruses* 14, 1999. doi:10.3390/v14091999

Funnell, S. G. P., Afrough, B., Baczenas, J. J., Berry, N., Bewley, K. R., Bradford, R., et al. (2021). A cautionary perspective regarding the isolation and serial propagation of SARS-CoV-2 in Vero cells. *NPJ Vaccines* 6, 83. doi:10.1038/s41541-021-00346-z

Graichen, H. (2021). What is the difference between the first and the second/third wave of Covid-19? - German perspective. *J. Orthop.* 24, A1–A3. doi:10.1016/j.jor.2021.01.011

Harcourt, J., Tamin, A., Lu, X., Kamili, S., Sakthivel, S. K., Murray, J., et al. (2020). Severe acute respiratory Syndrome coronavirus 2 from patient with coronavirus disease, United States. *Emerg. Infect. Dis.* 26, 1266–1273. doi:10.3201/eid2606.200516

Haslwanter, D., Dieterle, M. E., Wec, A. Z., O'Brien, C. M., Sakharkar, M., Florez, C., et al. (2021). A combination of receptor-binding domain and N-terminal domain neutralizing antibodies limits the generation of SARS-CoV-2 spike neutralization-escape mutants. *mBio* 12, e0247321. doi:10.1128/mBio.02473-21

Heyer, A., Gunther, T., Robitaille, A., Lutgehetmann, M., Addo, M. M., Jarczak, D., et al. (2022). Remdesivir-induced emergence of SARS-CoV2 variants in patients with prolonged infection. *Infect. Cell Rep. Med.* 3, 100735. doi:10.1016/j.xcrm.2022.100735

Honigberg, L. A., Smith, A. M., Sirisawad, M., Verner, E., Loury, D., Chang, B., et al. (2010). The Bruton tyrosine kinase inhibitor PCI-32765 blocks B-cell activation and is efficacious in models of autoimmune disease and B-cell malignancy. *Proc. Natl. Acad. Sci. U. S. A.* 107, 13075–13080. doi:10.1073/pnas.1004594107

Hussain, A., Hasan, A., Nejadi Babadaei, M. M., Bloukh, S. H., Chowdhury, M. E. H., Sharifi, M., et al. (2020). Targeting SARS-CoV2 spike protein receptor binding domain by therapeutic antibodies. *Biomed. Pharmacother.* 130, 110559. doi:10.1016/j.biopha.2020.110559

Ianevski, A., Giri, A. K., and Aittokallio, T. (2022). SynergyFinder 3.0: an interactive analysis and consensus interpretation of multi-drug synergies across multiple samples. *Nucleic Acids Res.* 50 (W1), W739–W743. doi:10.1093/nar/gkac382

Jeon, S., Ko, M., Lee, J., Choi, I., Byun, S. Y., Park, S., et al. (2020). Identification of antiviral drug candidates against SARS-CoV-2 from FDA-approved drugs. *Agents Chemother.* 64, e00819–e00820. doi:10.1128/AAC.00819-20

Jia, Z., and Gong, W. (2021). Will mutations in the spike protein of SARS-CoV-2 lead to the failure of COVID-19 vaccines? *J. Korean Med. Sci.* 36, e124. doi:10.3346/jkms.2021.36.e124

Johns Hopkins University(JHU) (2020). COVID-19 dashboard by the center for systems science and engineering (CSSE)

Kandeel, M., Abdelrahman, A. H. M., Oh-Hashi, K., Ibrahim, A., Venugopala, K. N., Morsy, M. A., et al. (2021). Repurposing of FDA-approved antivirals, antibiotics, anthelmintics, antioxidants, and cell protectives against SARS-CoV-2 papain-like protease. *J. Biomol. Struct. Dyn.* 39, 5129–5136. doi:10.1080/07391102.2020.1784291

Kinoshita, K., Asoh, K., Furuichi, N., Ito, T., Kawada, H., Hara, S., et al. (2012). Design and synthesis of a highly selective, orally active and potent anaplastic lymphoma kinase inhibitor (CH5424802). *Bioorg Med. Chem.* 20, 1271–1280. doi:10.1016/j.bmc.2011.12.021

Kumar, S., Sarma, P., Kaur, H., Prajapat, M., Bhattacharyya, A., Avti, P., et al. (2021). Clinically relevant cell culture models and their significance in isolation, pathogenesis, vaccine development, repurposing and screening of new drugs for SARS-CoV-2: a systematic review. *a Syst. Rev. Tissue Cell* 70, 101497. doi:10.1016/j.tice.2021.101497

Lamprecht, M. R., Sabatini, D. M., and Carpenter, A. E. (2007). CellProfiler: free, versatile software for automated biological image analysis. *Biotechniques*. 42, 71–75. doi:10.2144/000112257

Li, Y., Renner, D. M., Comar, C. E., Whelan, J. N., Reyes, H. M., Cardenas-Diaz, F. L., et al. (2021). SARS-CoV-2 induces double-stranded RNA-mediated innate immune responses in respiratory epithelial-derived cells and cardiomyocytes. *Proc. Natl. Acad. Sci. U. S. A.* 118, e2022643118. doi:10.1073/pnas.2022643118

Liu, X., Verma, A., Garcia, G., Jr., Ramage, H., Lucas, A., Myers, R. L., et al. (2021). Targeting the coronavirus nucleocapsid protein through GSK-3 inhibition. *Proc. Natl. Acad. Sci. U. S. A.* 118, e2113401118. doi:10.1073/pnas.2113401118

Londres, H. D., Armada, J. J., Martinez, A. H., Abdo Cuza, A. A., Sanchez, Y. H., Rodriguez, A. G., et al. (2022). Blocking EGFR with nimotuzumab: a novel strategy for COVID-19 treatment. *Immunotherapy* 14, 521–530. doi:10.2217/imt-2022-0027

Mateo, J., Ganji, G., Lemech, C., Burris, H. A., Han, S. W., Swales, K., et al. (2017). A first-time-in-human study of GSK2636771, a phosphoinositide 3 kinase beta-selective inhibitor, in patients with advanced solid tumors. *Clin. Cancer Res.* 23, 5981–5992. doi:10.1158/1078-0432.CCR-17-0725

Mautner, L., Hoyos, M., Dangel, A., Berger, C., Ehrhardt, A., and Baiker, A. (2022). Replication kinetics and infectivity of SARS-CoV-2 variants of concern in common cell culture models. *Virol. J.* 19, 76. doi:10.1186/s12985-022-01802-5

McCallum, M., De Marco, A., Lempp, F. A., Tortorici, M. A., Pinto, D., Walls, A. C., et al. (2021). N-terminal domain antigenic mapping reveals a site of vulnerability for SARS-CoV-2. *Cell* 184 (03.028), 2332–2347.e16. 2332-2347 e2316. doi:10.1016/j.cell.2021.03.028

McInnes, L., Healy, J., and Melville, J. (2018). UMAP: uniform manifold approximation and projection for dimension reduction. *arXiv*. doi:10.48550/arXiv.1802.03426

McLean, G., Kamil, J., Lee, B., Moore, P., Schulz, T. F., Muik, A., et al. (2022). The impact of evolving SARS-CoV-2 mutations and variants on COVID-19 vaccines. *mBio* 13, e0297921. doi:10.1128/mbio.02979-21

Mullen, P. J., Garcia, G., Jr., Purkayastha, A., Matulionis, N., Schmid, E. W., Momcilovic, M., et al. (2021). SARS-CoV-2 infection rewires host cell metabolism and is potentially susceptible to mTORC1 inhibition. *Nat. Commun.* 12, 1876. doi:10.1038/s41467-021-22166-4

Ngan, D. K., Xu, T., Xia, M., Zheng, W., and Huang, R. (2022). Repurposing drugs as COVID-19 therapies: a toxicity evaluation. *A Toxic. Eval. Drug Discov. Today* 27, 1983–1993. doi:10.1016/j.drudis.2022.04.001

Ogando, N. S., Dalebout, T. J., Zevenhoven-Dobbe, J. C., Limpens, R., van der Meer, Y., Caly, L., et al. (2020). SARS-coronavirus-2 replication in Vero E6 cells: replication kinetics, rapid adaptation and cytopathology. *J. Gen. Virol.* 101, 925–940. doi:10.1099/jgv.0.001453

Owen, D. R., Allerton, C. M. N., Anderson, A. S., Aschenbrenner, L., Avery, M., Berritt, S., et al. (2021). An oral SARS-CoV-2 M(pro) inhibitor clinical candidate for the treatment of COVID-19. *Science* 374 (6575), 1586–1593. doi:10.1126/science.abl4784

Rathnasinghe, R., Jangra, S., Cupic, A., Martinez-Romero, C., Mulder, L. C. F., Kehrer, T., et al. (2021). The N501Y mutation in SARS-CoV-2 spike leads to morbidity in obese and aged mice and is neutralized by convalescent and post-vaccination human sera. medRxiv, 2021.01.19.21249592. doi:10.1101/2021.01.19.21249592

Sakamoto, H., Tsukaguchi, T., Hiroshima, S., Kodama, T., Kobayashi, T., Fukami, T. A., et al. (2011). CH5424802, a selective ALK inhibitor capable of blocking the resistant gatekeeper mutant. *Cancer Cell* 19, 679–690. doi:10.1016/j.ccr.2011.04.004

Sola, I., Almazan, F., Zuniga, S., and Enjuanes, L. (2015). Continuous and discontinuous RNA synthesis in coronaviruses. *Coronaviruses Annu. Rev. Virol.* 2, 265–288. doi:10.1146/annurev-virology-100114-055218

Soriano, V., de Mendoza, C., Gomez-Gallego, F., Corral, O., and Barreiro, P. (2021b). Third wave of COVID-19 in Madrid, Spain. *Int. J. Infect. Dis.* 107, 212–214. doi:10.1016/j.ijid.2021.04.074

Soriano, V., Ganado-Pinilla, P., Sanchez-Santos, M., Gomez-Gallego, F., Barreiro, P., de Mendoza, C., et al. (2021a). Main differences between the first and second waves of COVID-19 in Madrid, Spain. *Int. J. Infect. Dis.* 105, 374–376. doi:10.1016/j.ijid.2021.02.115

Stadler, K., Masignani, V., Eickmann, M., Becker, S., Abrignani, S., Klenk, H. D., et al. (2003). SARS–beginning to understand a new virus. *Nat. Rev. Microbiol.* 1, 209–218. doi:10.1038/nrmicro775

Stirling, D. R., Swain-Bowden, M. J., Lucas, A. M., Carpenter, A. E., Cimini, B. A., and Goodman, A. (2021). CellProfiler 4: improvements in speed, utility and usability. *BMC Bioinforma.* 22, 433. doi:10.1186/s12859-021-04344-9

Tai, W., He, L., Zhang, X., Pu, J., Voronin, D., Jiang, S., et al. (2020). Characterization of the receptor-binding domain (RBD) of 2019 novel coronavirus: implication for development of RBD protein as a viral attachment inhibitor and vaccine. *Mol. Immunol.* 17, 613–620. doi:10.1038/s41423-020-0400-4

Thorne, C. A., Chen, I. W., Sanman, L. E., Cobb, M. H., Wu, L. F., and Altschuler, S. J. (2018). Enteroid monolayers reveal an autonomous WNT and BMP circuit controlling intestinal epithelial growth and organization. *Dev. Cell* 44, 624–633. doi:10.1016/j.devcel.2018.01.024

Touret, F., Giraud, E., Bourret, J., Donati, F., Tran-Rajau, J., Chiaravalli, J., et al. (2023). Enhanced neutralization escape to therapeutic monoclonal antibodies by SARS-CoV-2 omicron sub-lineages. *iScience* 26, 106413. doi:10.1016/j.isci.2023.106413

VanBlargan, L. A., Errico, J. M., Halfmann, P. J., Zost, S. J., Crowe, J. E., Jr., Purcell, L. A., et al. (2022). An infectious SARS-CoV-2 B.1.1.529 Omicron virus escapes neutralization by therapeutic monoclonal antibodies. *Nat. Med.* 28, 490–495. doi:10.1038/s41591-021-01678-y

Wang, M., Cao, R., Zhang, L., Yang, X., Liu, J., Xu, M., et al. (2020). Remdesivir and chloroquine effectively inhibit the recently emerged novel coronavirus (2019-nCoV) *in vitro*. *Cell Res.* 30, 269–271. doi:10.1038/s41422-020-0282-0

Weinreich, D. M., Sivapalasingam, S., Norton, T., Ali, S., Gao, H., Bhore, R., et al. (2021). REGN-COV2, a neutralizing antibody cocktail, in outpatients with covid-19. *N. Engl. J. Med.* 384, 238–251. doi:10.1056/NEJMoa2035002

Weisberg, E., Parent, A., Yang, P. L., Sattler, M., Liu, Q., Liu, Q., et al. (2020). Repurposing of kinase inhibitors for treatment of COVID-19. *Pharm. Res.* 37, 167. doi:10.1007/s11095-020-02851-7

Weston, S., Coleman, C. M., Haupt, R., Logue, J., Matthews, K., Li, Y., et al. (2020). Broad anti-coronavirus activity of food and drug administration-approved drugs against SARS-CoV-2 *in vitro* and SARS-CoV *in vivo*. *J Virol* 94, e01218–e01220. doi:10.1128/JVI.01218-20

Yang, F., Chen, R., Li, W. Y., Zhu, H. Y., Chen, X. X., Hou, Z. F., et al. (2021). D-limonene is a potential monoterpene to inhibit PI3K/Akt/IKK-α/NF-κB p65 signaling pathway in coronavirus disease 2019 pulmonary fibrosis. *Front. Med. (Lausanne)* 8, 591830. doi:10.3389/fmed.2021.591830

Zaki, A. M., van Boheemen, S., Bestebroer, T. M., Osterhaus, A. D., and Fouchier, R. A. (2012). Isolation of a novel coronavirus from a man with pneumonia in Saudi Arabia. *Saudi Arab. N. Engl. J. Med.* 367, 1814–1820. doi:10.1056/NEJMoa1211721

Zost, S. J., Gilchuk, P., Case, J. B., Binshtein, E., Chen, R. E., Nkolola, J. P., et al. (2020b). Potently neutralizing and protective human antibodies against SARS-CoV-2. *Nature* 584, 443–449. doi:10.1038/s41586-020-2548-6

Zost, S. J., Gilchuk, P., Chen, R. E., Case, J. B., Reidy, J. X., Trivette, A., et al. (2020a). Rapid isolation and profiling of a diverse panel of human monoclonal antibodies targeting the SARS-CoV-2 spike protein. *Nat. Med.* 26, 1422–1427. doi:10.1038/s41591-020-0998-x